# Quantum flux studies of the mechanism of Ca(4s5p 1 P)→Ca(4s5p 3 P) collisions

Millard H. Alexander

Citation: The Journal of Chemical Physics **96**, 6672 (1992); doi: 10.1063/1.462606
View online: http://dx.doi.org/10.1063/1.462606
View Table of Contents: http://scitation.aip.org/content/aip/journal/jcp/96/9?ver=pdfcov
Published by the AIP Publishing

# Quantum flux studies of the mechanism of Ca($4s5p\ ^1P$)→Ca($4s5p\ ^3P$) collisions

Millard H. Alexander
*Department of Chemistry and Biochemistry, University of Maryland, College Park, Maryland 20742*

(Received 18 October 1991; accepted 13 January 1992)

We apply a new method [M. H. Alexander, J. Chem. Phys. **94**, 8931 (1991)] for the study of the mechanism of inelastic collisions, to the analysis of spin-changing collisions of Ca atoms in the $4s5p$ Rydberg state. The method involves the determination of the current density associated with, separately, the incoming and outgoing scattering wave functions in a locally adiabatic basis. This yields a picture of how the incoming flux, initially associated with a given internal state, redistributes itself as a function of the interparticle separation both as the particles approach, and, subsequently, as the particles recede. By proper selection of the initial state, we explore the dependence on orbital orientation of the probability for the spin-changing Ca($4s5p\ ^1P$)→Ca($4s5p\ ^3P$) process. Further, we show how the distribution of population among the fine-structure levels of the $^3P$ state depends on final-state interactions in the exit channel.

## I. INTRODUCTION

There has been considerable recent theoretical interest in the influence of orbital alignment on the efficiency of spin-changing collisions involving atoms in $P$ electronic states.[1-5] This work has been motivated by the experimental study by Leone and co-workers[6-11] of spin-changing transitions between the $^1P$ and $^3P$ electronic states of the $4s5p$ Rydberg levels of Ca induced by collisions with a variety of atomic and molecular targets.

Qualitatively, spin-changing $^1P\rightarrow{}^3P$ transitions involving Ca($4s5p$) atoms can be understood easily in terms of the electronic potential curves which correlate with the $^1P$ and $^3P$ Ca + He asymptotes, as illustrated in Fig. 1. At long range it is appropriate to use a Hund's case (e) description,[12-14] in which the states are labeled by the total electronic angular momentum of the atom, $j$, and the orbital angular momentum associated with the relative motion of the collision partners, $l$. At short range it is appropriate to use a Hund's case (a) basis[15,16] in which the states are labeled by $\Lambda$, the projection of the electronic orbital angular momentum $L$ along the molecular (body-frame) axis, and by the total angular momentum $J$. The threefold orbital degeneracy of a $P$ state atom is split by the perturber atom, giving rise to two degenerate electronic potential curves of $\Pi$ symmetry, and one curve of $\Sigma$ symmetry. The curves of $\Pi$ symmetry are expected to be less repulsive, since they correspond to a situation in which the $p$ orbital is oriented perpendicular to $R$, the Ca–He axis.

Spin changing transitions occur by means of the small, off diagonal in $S$, spin–orbit mixing[16] which becomes significant at the point at which the $^1\Pi$ curve is crossed by the more repulsive $^3\Sigma$ curve, which correlates with the lower $^3P$ asymptote (Fig. 1). The motivation behind the original experiments of Leone was that by varying the polarization vector of the laser used to populate initially the Ca($4s5p\ ^1P$) state, one could control the distribution of collision flux between the $^1\Pi$ and $^1\Sigma$ curves in Fig. 1 and thereby control the amount of flux which reached the singlet–triplet curve crossing leading to $^3P$ products.

We have subsequently reported[1,2] the results of fully-quantum studies of the inelastic $^1P\leftrightarrow{}^3P$ processes under investigation in Leone's group. Unfortunately, these (as all) close-coupling calculations, despite yielding values of the relevant cross sections and polarization ratios which agreed well with experiment, offered little physical insight into the dependence on initial orbital alignment of the cross sections into the various $^3P_j$ final states. Subsequently, using the proper description of the initial state, as clarified by Schatz, Kovalenko, Delos, and Leone,[3,4] we carried out[5] a study of the collisional reorientation of the initially prepared $p$ orbital in the entrance ($^1P$) channel. The primary focus of that paper[5] was the quantum interpretation of the earlier concept of "orbital locking" introduced by Hertel, Grosser, and their colleagues.[17-20] Little attempt was made to analyse in detail the mechanism of the spin-changing $^3P\rightarrow{}^1P$ process.

In a recent article[21] we have shown how the standard, time-independent, close-coupled (CC) formulation of inelastic scattering[22-24] could be extended to the study of actual mechanisms of inelastic processes. Hitherto, it was thought that a major drawback of time-independent CC calculations was that information on the transfer of flux from a particular initial state to a given final state was readily accessible only asymptotically, at large interparticle separations, after the collision is finished. Thus little "mechanistic" insight could be obtained. Our new extension involves the determination, as a function of interparticle separation, of the redistribution of the incoming inelastic flux among the various internal quantum states of the system in a locally adiabatic basis, both as the particles approach and as they recede. This allows one to investigate the progressive transfer of the initial flux associated with a particular internal state into the other internal states which are coupled to the initial state in question. Similarly, determination of the outgoing flux as a function of the interparticle separation gives information on how quickly the distribution among internal states relaxes



 0021-9606/92/096672-09$06.00 

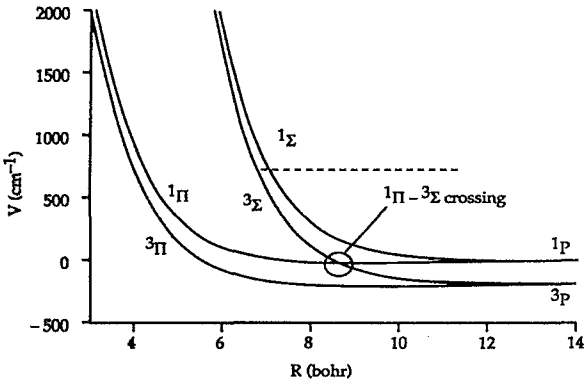


FIG. 1. Typical potential energy curves of $^1\Sigma$, $^3\Sigma$, $^1\Pi$, and $^3\Pi$ symmetry which would arise from the interaction of a closed-shell atom with an atom in ($\cdots nsn'p\ ^1P$) and ($\cdots nsn'p\ ^3P$) electronic states. The actual potential energy curves shown are appropriate to the interaction of Ca(4s5p) with He and are taken from Ref. 2. The dashed line indicates an energy of 246 mhartree (540 cm$^{-1}$) relative to the $^1P$ state, which is the energy used in the calculations to be described below. Also shown is the crossing between the $^1\Pi$ and $^3\Sigma$ curves, by means of which $^1P \rightarrow ^3P$ transitions take place.

into the asymptotic distribution, as would be determined in a conventional CC calculation.

In the present article we shall apply our new method for the quantum study of the redistribution of collision flux to spin changing collisions involving Ca(4s5p) atoms, specifically the process.

$$\mathrm{Ca}(4s5p\ ^1P) + \mathrm{He} \rightarrow \mathrm{Ca}(4s5p\ ^3P) + \mathrm{He}. \tag{1}$$

Our goals will be the investigation of (1) how the orientation of the initially excited 5p orbital governs the transfer to the manifold of $^3P$ states and (2) at what interparticle distance does the distribution of populations among the three fine structure levels of the $^3P$ atom become established. The organization of the present article is as follows: In the next section we review briefly our recently introduced[21] technique for the study of the redistribution of flux. In Sec. III we summarize the relevant aspects of the quantum description of the spin-changing process of Eq. (1). Sections IV and V summarize the flux redistribution for collisions at small and large impact parameters. A brief conclusion follows.

## II. DETERMINATION OF THE COLLISION FLUX

In the quantum description of inelastic collisions between particles with internal degrees of freedom, the standard technique for the solution of the time-independent Schrödinger equation involves expansion in a complete set of states in the internal degrees of freedom. The expansion coefficients, which depend implicitly on the separation between the two particles, are solutions to a set of ordinary differential equations, the "close-coupled" (CC) equations.[22–24] By analysis of the asymptotic form of these solutions, one obtains the $S$ matrix, which contains all the dynamically relevant information.

The general structure of the close-coupled equations can be expressed by the matrix equation

$$[\mathbf{1}d^2/dR^2 + \mathbf{W}(R)]\mathbf{F}(R) = 0. \tag{2}$$

Here $R$ designates the interparticle separation, $\mathbf{1}$ is the identity matrix, and the matrix $\mathbf{W}(R)$ includes the (full, symmetric) matrix of the coupling potential as well as the diagonal matrices of the centrifugal potential and the translational energy associated with each internal state (channel). This W matrix is expressed in a basis which is the product space of the internal states of the isolated collision partners, which we denote as $|\mathbf{d}\rangle$. Alternatively, a fully adiabatic basis $|\mathbf{a}\rangle$ can be defined,[25,26] by an orthogonal transformation of the diabatic basis, namely,

$$|\mathbf{a}\rangle = \mathbf{T}(R)|\mathbf{d}\rangle. \tag{3}$$

The transformation matrix is chosen to diagonalize the matrix of the total Hamiltonian

$$\mathbf{T}(R)\mathbf{W}(R)\mathbf{T}^T(R) = \boldsymbol{\lambda}(R) \equiv -\mathbf{k}^2(R), \tag{4}$$

where $\boldsymbol{\lambda}(R)$ is the (diagonal) matrix of eigenvalues, and $\mathbf{k}^2(R)$ is the diagonal wave vector matrix. Asymptotically, the $j^{\text{th}}$ element of this matrix is the wave vector associated with the $j^{\text{th}}$ channel.

At large $R$, the solutions which are regular at the origin can be written as

$$\mathbf{F}(R) = \mathbf{F}_i(R) + \mathbf{F}_o(R), \tag{5}$$

where the subscripts designate incoming and outgoing waves and

$$\lim_{R\rightarrow\infty} \mathbf{F}_i(R) = \mathbf{I}(R), \tag{6a}$$

and

$$\lim_{R\rightarrow\infty} \mathbf{F}_o(R) = \mathbf{O}(R)\mathbf{S}, \tag{6b}$$

where $\mathbf{S}$ designates the scattering matrix and $\mathbf{I}$ and $\mathbf{O}$ are diagonal matrices with elements proportional to Ricatti–Hankel functions.[5,21] The $k^{\text{th}}$ column of the solution matrix $\mathbf{F}(R)$ is the particular scattering wave function corresponding to incoming flux in the $k^{\text{th}}$ internal state. The $j^{\text{th}}$ row represents the component of internal state $|j\rangle$ in this wave function

We also define a *flux matrix* $\mathbf{J}(R)$ whose $jk^{\text{th}}$ element is the flux (current density) in internal state $j$ at internuclear separation $R$, corresponding to incoming flux of magnitude $\hbar/\mu$ in internal state $k$, namely,

$$[\mathbf{J}(R)]_{jk} = (i\hbar/2\mu)\{\mathbf{F}(R)\cdot\mathbf{F}'(R)^* - \text{c.c.}\}_{jk}. \tag{7}$$

Here $\mathbf{F}'$ designates the first derivative of the solution matrix with respect to $R$ and the multiplication is taken to mean element-by-element multiplication rather than a matrix product. Our definition of the flux here is consistent with the convention that a *negative* sign corresponds to flux directed inward (toward decreasing $R$).

Formally, one can separate the flux into incoming and outgoing components

$$\mathbf{J}(R) = \mathbf{J}_i(R) + \mathbf{J}_o(R), \tag{8}$$

where

$$[\mathbf{J}_i(R)]_{jk} = (i\hbar/2\mu)\{\mathbf{F}_i(R)\cdot(d/dR)\mathbf{F}_i(R)^* - \text{c.c.}\}_{jk}, \tag{9}$$

with a similar equation for the outgoing flux. Asymptotically,

$$\lim_{R\to\infty}[\mathbf{J}_i(R)]_{jk} = -\hbar\delta_{jk}/\mu \tag{10a}$$

and

$$\lim_{R\to\infty}[\mathbf{J}_o(R)]_{jk} = \hbar|S_{jk}|^2/\mu. \tag{10b}$$

We have shown[21] that the separation of the collision flux into incoming and outgoing components remains valid as the value of $R$ decreases; in other words that the flux associated initially with the incoming wave can be determined solely from the incoming wave at all values of $R$ (and similarly for the flux associated with the outgoing wave) and that at any value of $R$ the *total* incoming or outgoing flux, summed over internal states, is separately conserved.

This technique provides a powerful means for analysis of the collision dynamics: As the two particles approach, the progressive transfer of the initial flux associated with a particular internal state into the other internal states is a probe of the region of interparticle separation over which the collision effectively couples pairs of internal states. Similarly, examination of the outgoing flux, again as a function of the interparticle distance, gives information on how quickly the distribution among internal states relaxes into the asymptotic distribution, as would be determined in a conventional CC calculation.

Rather than refer to the asymptotic basis, in which the CC equations are formulated, it is more meaningful to examine the redistribution of flux in the *adiabatic* basis, since the adiabatic states are the local eigenstates of the system, as a function of the interparticle separation. Transfer of flux between adiabatic states is a measure of the extent to which the collision occurs too quickly for the system to follow adiabatically.

The actual determination of the flux matrix is a straightfoward extension of available techniques for the solution of the CC equations. The salient features are summarized below; for more detail the reader is referred to our earlier paper.[21]

Numerical solution of the CC equations involves breaking up the range of integration into a number of sectors. One of the most stable and efficient algorithms for propagation across a sector is the log-derivative method.[24,27-32] Here, the wave function and its derivative at either side of each sector are related by

$$\begin{bmatrix}\mathbf{F}'(R_{m-1})\\ \mathbf{F}'(R_m)\end{bmatrix} = \begin{bmatrix}\mathbf{L}_1^{(m)} & \mathbf{L}_2^{(m)}\\ \mathbf{L}_3^{(m)} & \mathbf{L}_4^{(m)}\end{bmatrix}\begin{bmatrix}-\mathbf{F}(R_{m-1})\\ \mathbf{F}(R_m)\end{bmatrix}, \tag{11}$$

where $R_{m-1}$ and $R_m$ define the sides of sector $m$ with $R_{m-1}<R_m$. In Eq. (11) each of the log-derivative propagators $\mathbf{L}_i^{(m)}$ is a matrix of dimension equal to the number of channels.

It follows that the solution matrix at the left-hand side of the sector is given in terms of its value and derivative at the right-hand side by

$$\mathbf{F}(R_{m-1}) = -[\mathbf{L}_3^{(m)}]^{-1}[\mathbf{F}'(R_m) - \mathbf{L}_4^{(m)}\mathbf{F}(R_m)]. \tag{12a}$$

With Eq. (11) and Eq. (12a) the derivative at the left hand side can be obtained directly as

$$\mathbf{F}'(R_{m-1}) = -\mathbf{L}_1^{(m)}\mathbf{F}(R_{m-1}) + \mathbf{L}_2^{(m)}\mathbf{F}(R_m). \tag{12b}$$

In our implementation[32] of the linear reference potential algorithm,[33,34] the $\mathbf{W}(R)$ matrix is diagonalized in each sector, which defines the transformation matrices $\mathbf{T}_m(R)$ to the locally adiabatic basis. Propagation across the sector is done in the locally adiabatic basis.

After determination of the $S$ matrix, Eq. (12) can be used to determine the wave function and its derivative, and, subsequently, the flux at each sector boundary, progressing *inwards* from the outermost value of $R$. This involves (1) transforming the wave function at the outer boundary of the sector into the locally adiabatic basis using the sector transformation matrix $\mathbf{T}_m$; (2) using Eq. (12) to determine the wave function and its derivative at the inner boundary of the sector (still in the locally adiabatic basis); determining the flux in the locally adiabatic basis at the inner boundary from Eq. (9); and then transforming the wave function at the inner boundary into the asymptotic basis using the transpose of the sector transformation matrix.

A simple stabilization procedure was introduced[21] to eliminate numerical contamination caused by the exponentially growing component in components of the wave function associated with closed channels: For any channel which is locally closed, the wave function and its derivative at the inner boundary of the sector ($R_{m-1}$) are damped according to the relation

$$f_j(R_{m-1}) = \exp(-\alpha^{(m)}|\lambda_j^{(m)}|^{1/2}\Delta_m)f_j^o(R_{m-1}), \tag{13}$$

where $f_j^o(R_{m-1})$ indicates the value which would have been predicted using the exact propagator relation. Here, $\lambda_j^{(m)}$ denotes the $j^{\text{th}}$ adiabatic eigenvalue in sector $m$, $\alpha^{(m)}$ is a constant, and $\Delta_m$ denotes the width of sector $m$.

## III. COLLISION DYNAMICS

The quantum description of spin-changing collisions between $^1P$ states of Ca and noble gases was presented in 1987 by Pouilly and Alexander[1] and further refined in subsequent articles.[2,5,35,36] We shall repeat here only directly relevant equations.

At large Ca–He distances it is most convenient to work with states obtained by vector coupling the wave function which describes the relative orbital motion of the two collision partners, $|lm_l\rangle$, and the state $|LSjm_j\rangle$ which describes the fine structure level of the atom. These Hund's case (e) states are given by

$$|LSjlJM\rangle = \sum_{m_j m_l}(jm_j lm_l|JM)|LSjm_j\rangle|lm_l\rangle, \tag{14}$$

where $(\cdots\cdot|\cdot\cdot)$ is a Clebsch–Gordan coefficient[37] and $M$ is the projection of the total angular momentum $J$ along a space-fixed $Z$ axis. For a $^1P$ state, $S=0$ and $L=1$, so that for a given $J$ there are two $e$-labeled[38] case (e) states, with parity $(-1)^J$, corresponding to $l=J\pm1$, and one $f$-labeled state, with parity $-(-1)^J$ and $l=J$.[35,36] At short range, the two $e$-labeled case (e) states correlate with the $^1\Pi_e$ and $^1\Sigma^+$ case (a) states, mentioned in the Sec. I. The sole $f$-labeled state correlates with the $^1\Pi_f$ state. The two $e$-labeled case (a) states ($^1\Sigma_e$ and $^1\Pi_e$) are coupled by the orbital motion of the two atomic collision partners.[5,16] For a $^3P$ state, $S=1$ and $L=1$, so that for a given $J$ there are four $e$-

labeled[38] case (e) states corresponding to $j=1,2; l=J\pm 1$, and five $f$-labeled states, corresponding to $j=2, l=J, J\pm 2$, and $j=1,0; l=J$. For brevity, we shall henceforth suppress the $L$ quantum number in the labeling of the case (e) states and use the notation $|SlJM\rangle$. At short range, the $e$-labeled case (e) states of triplet multiplicity correlate with the $^3\Pi_{\Omega=0,1,2,e}$ and $^3\Sigma_{\Omega=1,e}$ case (a) states while the $f$-labeled case (e) states correlate with the $^3\Pi_{\Omega=0,1,2,f}$ and $^3\Sigma_{\Omega=0,1,f}$ case (a) states.

When the electric field vector of the excitation laser (assumed linearly polarized) is directed parallel to the initial relative velocity vector, the initial state can be constructed, following Schatz and co-workers,[4] as the product of an incoming plane wave in the relative motion of the Ca and He atoms, multiplied by the electronic wave function of the atom, $|S=0,L=1,M_L=0\rangle$. We have shown[5] that this is equivalent to the following coherent sum of only $e$-labeled case (e) states:

$$\lim_{R\to\infty}\Psi_{\|}(R)=\frac{i\pi^{1/2}}{2kR}\sum_{J=1}^{\infty}(-1)^J[(-1)^J e^{ikR}+e^{-ikR}]\times[(J+1)^{1/2}|S=0,J+1,J0\rangle-J^{1/2}|S=0,J-1,J0\rangle]. \quad (15)$$

As we have demonstrated,[5] this is equivalent to preparation of a pure $^1\Sigma_e$ state.

In the case that the electric field vector of the excitation laser is aligned perpendicular to the relative velocity vector, the two electronic states $|S=0,L=1,M_L=+1\rangle$ and $|S=0,L=1,M_L=-1\rangle$ (or, equivalently, the $\Lambda$-doublet pair, $^1\Pi_e$ and $^1\Pi_f$) are prepared with equal probability. Asymptotically, the $e$-labeled component must be orthogonal to the $e$-labeled state defined by Eq. (15) and can therefore be written as

$$\lim_{R\to\infty}\Psi_{e\perp}(R)=\frac{i\pi^{1/2}}{2kR}\sum_{J=1}^{\infty}(-1)^J[(-1)^J e^{ikR}+e^{-ikR}]\times[-J^{1/2}|S=0,J+1,J0\rangle-(J+1)^{1/2}|S=0,J-1,J0\rangle]. \quad (16)$$

For the $f$-labeled component under parallel excitation there are no coherences with the purely $e$-labeled state corresponding to perpendicular excitation. Thus a conventional close-coupled analysis[1] in a coupled (total $J$) basis can be made in which the system is prepared in the single case (e) state with $L=1$, $S=0$, $l=J$.[35]

The calculations to be described used the model $^{1,3}\Pi$ and $^{1,3}\Sigma$ Ca–He potential curves given by Pouilly *et al.*,[2] although more recent pseudopotential curves have been published by Czuchaj and co-workers.[39,40] The scattering calculations were carried out at an initial energy in the $^1P$ state of 540 cm$^{-1}$. For this energy partial cross sections for transitions from the $^1P_{1f}$ to the $^3P_{J=0,1,2}$ levels, summed over the projection degeneracy of the final state, are displayed in Fig. 2. The integral cross sections are defined in terms of these partial cross sections by

$$\sigma(^1P\to{}^3P_j)=\sum_J \sigma_J(^1P\to{}^3P_j). \quad (17)$$

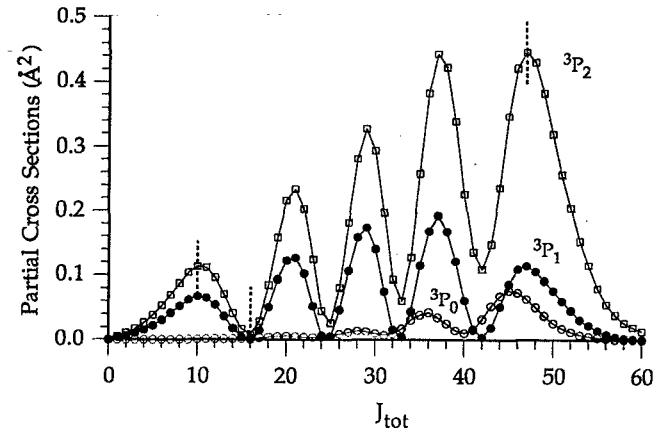


FIG. 2. Partial cross sections [Eq. (17), in Å$^2$] as a function of the total angular momentum $J_{tot}$ for Ca($4s5p\ ^1P\to{}^3P$) transitions in collisions with He at an energy of 246 mhartree (540 cm$^{-1}$). The potential curves used are those shown in Fig. 1 The partial cross sections shown are averaged over all three $^1P_{mj}$ initial states and are thus appropriate to a cell experiment (Ref. 6) in which the alignment of the $5p$ orbital is not selected. Indicated with vertical dashed lines are the three values of $J_{tot}$ (10,16,47) for which the analysis of the incoming and outgoing fluxes was carried out.

The semiclassical interpretation[25,26] of the oscillatory structure in Fig. 2 involves interference between trajectories which undergo the singlet→triplet crossing as the atoms approach or as they recede; in a semiclassical sense these two processes interfere constructively or destructively as the phase difference between these two trajectories is modulated by the shift in the potentials due to the increasing centrifugal barrier.

## IV. FLUX TRANSFER, SMALL IMPACT PARAMETER

We first consider collisions at a total angular momentum of $J_{tot}=10$. This corresponds to the first peak in the inelastic partial cross sections shown in Fig. 2. The six adiabatic potential curves associated with the $f$-labeled levels are shown in the upper panel of Fig. 3. The dominant spin–orbit mixing involves the $^1\Pi_{1f}$ and $^3\Sigma_{1f}$ states, which correlate asymptotically with the $^1P_{1f}$ and $^3P_{2f}$ levels, respectively. Note that there is no direct spin–orbit coupling between the singlet state and the $^3\Sigma_{0f}$ state,[1,2,36] since the selection rule for the spin–orbit operator is $\Delta\Omega=0$.[15,16] On the figure is indicated the avoided crossing between the $^1\Pi_{1f}$ and $^3\Sigma_{1f}$ curves, as well as the region of "radial coupling"[26,41,42] at which point the splitting between the $^3\Sigma$ and $^3\Pi$ curves becomes comparable to the fine structure splittings in the $^3P$ state of the isolated Ca atom (7 cm$^{-1}$ between the $^3P_0$ and $^3P_1$ levels and 28 cm$^{-1}$ between the $^3P_1$ and $^3P_2$ levels[43]).

Figure 4 displays the incoming and outgoing flux corresponding to initial excitation of the $^1P_{1f}$ state for $J_{tot}=10$ and $E_{col}=540$ cm$^{-1}$. As one might anticipate from the adiabatic energy curves in Fig. 3, transfer of flux out of the initial state ($n=6$) occurs almost exclusively to the $n=4$ state, which is the only state which is directly coupled with the initial state by the spin–orbit operator. Here, and in the succeeding text, we shall label the adiabatic states with the index $n$ in order of increasing energy. By contrast, only rela-

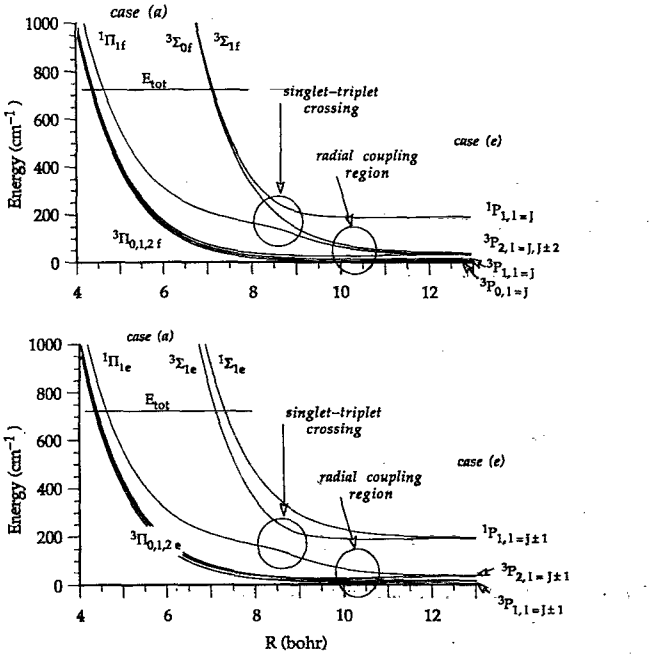


FIG. 3. (Upper panel) Dependence on internuclear distance of the six $f$-labeled adiabatic potential curves for the collision of Ca($4s5p$ $^{1,3}P$) with He for $J_{tot} = 10$. The curves are designated by appropriate Hund's case (a) and case (e) labeling [valid at small and large $R$, respectively (see Refs. 2 and 36)]. The underlying electronic potential curves were taken from Ref. 2 and are shown in Fig. 1. The region of strong spin–orbit mixing between the $^1\Pi_{1f}$ and $^3\Sigma_{1f}$ curves is shown, as is the region of "radial coupling" (Refs. 26, 41, and 42) at which point the splitting between the $^3\Sigma$ and $^3\Pi$ curves becomes comparable to the fine structure splittings in the $^3P$ state of the isolated Ca atom. The crossing region is traversed by the $^3\Sigma_{0f}$ curve, which is not spin–orbit coupled to the $^1\Pi_{1f}$ curve. The horizontal line indicates the value of the total energy for which the flux analysis was carried out. (Lower panel) Similar to the upper panel except that the $e$-labeled curves are displayed.

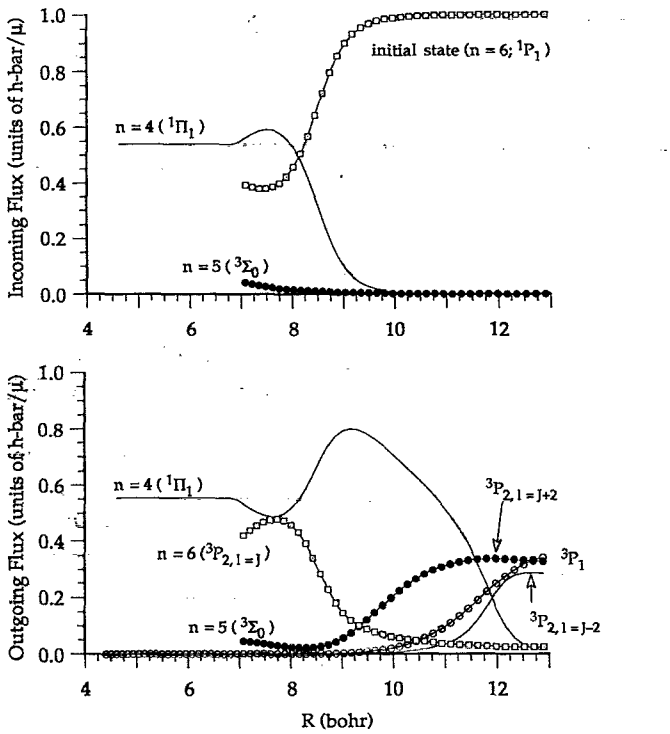


FIG. 4. (Upper panel) Redistribution of incoming flux among the various adiabatic $f$-labeled states of the Ca($4s5p$ $^{1,3}P$) He system (see Fig. 3) at an energy in the $^1P$ state of 540 cm$^{-1}$ and $J_{tot} = 10$. The initial state, with flux indicated by the open squares, is $n = 6$ ($^1P_{1f}$). The fluxes in the various adiabatic states are plotted only up to the classical turning points for these states. The incoming flux in the $n = 1$, 2, and 3 states is negligibly small on the scale of the figure. (Lower panel) Identical to the upper panel except that the outgoing flux is plotted. The outgoing flux in the $^3P_{0f}$ state ($n = 1$) is found to be negligibly small.

tively little flux transfer occurs to the $n = 5$ state, since this state correlates with the Hund's case (a) $^3\Sigma_{0f}$ state which is not directly coupled with the $^1\Pi_{1f}$ state. The corresponding outgoing flux is displayed in the lower panel of this figure. We see that the transfer of flux from the $^1P$ to the $n = 4$ (triplet) state occurs roughly equally as the particles approach and again as they recede. Also, almost no flux remains in the initial ($n = 6$) state after the collision is over, which indicates that at $J_{tot} = 10$, transfer out of the $^1P_{1f}$ state is nearly complete.

We also observe that the distribution among the $^3P_j$ spin–orbit states is established not at the curve crossing with the singlet state but only as the particles recede through the "radial coupling" region. The $n = 4$ triplet state, which is dominantly populated initially, loses almost all its flux to other $^3P_2$ and $^3P_1$ states. We also observe the virtual absence of flux transfer from the $^1P_{1f}$ state into the $^3P_0$ state. In the molecular region the $^3P_0$ state correlates with the $^3\Pi_0$ state (see Fig. 3), which is not directly coupled to the initially populated $^1\Pi_{1f}$ state. Thus, as discussed by Pouilly *et al.*,[2] population of the $^3P_0$ state will occur only through second-order processes involving Coriolis coupling between the $^3\Pi_0$ and $^3\Pi_1$ molecular states which correlate with the $^3P_{J=1,2}$ atomic states.

Figure 5 displays the incoming and outgoing fluxes corresponding to initial excitation of the $^1P_e$ state for $J_{tot} = 10$ and $E_{col} = 540$ cm$^{-1}$. Here we assume that the electric field vector is aligned *parallel* to the initial relative velocity vector so that the initial excitation produces the linear combination of the two $^1P_e$, $l = J \pm 1$ states described by Eq. (15). As illustrated in Fig. 6, on intuitive grounds one would expect that at small impact parameter excitation of the $5p$ orbital initially lying parallel to the relative velocity vector should induce preferential population of the $^1\Sigma$ potential (Fig. 1). We observe that the prediction of this intuitive picture is borne out by the flux calculations: the incoming flux, split initially between the two $^1P_e$, $l = J \pm 1$ states described by Eq. (15), is transferred progressively to the $n = 6$ adiabatic state which corresponds at short range to the $^1\Sigma_e$ state. Consequently, transfer to the adiabatic states of triplet multiplicity is minimal. As the particles recede (lower panel of Fig. 5) the flux reverts back to the linear combination of the two $^1P_e$ states initially excited.

By contrast, the initially prepared $^1P_e$ state arising from *perpendicular* excitation of the $5p$ orbital should lead to population of the $^1\Pi_e$ potential (Fig. 6) with subsequent population of the triplet states by means of the singlet–triplet crossing. This intuitive picture is again borne out by the quantum flux calculations, displayed in Fig. 7. The incoming flux is

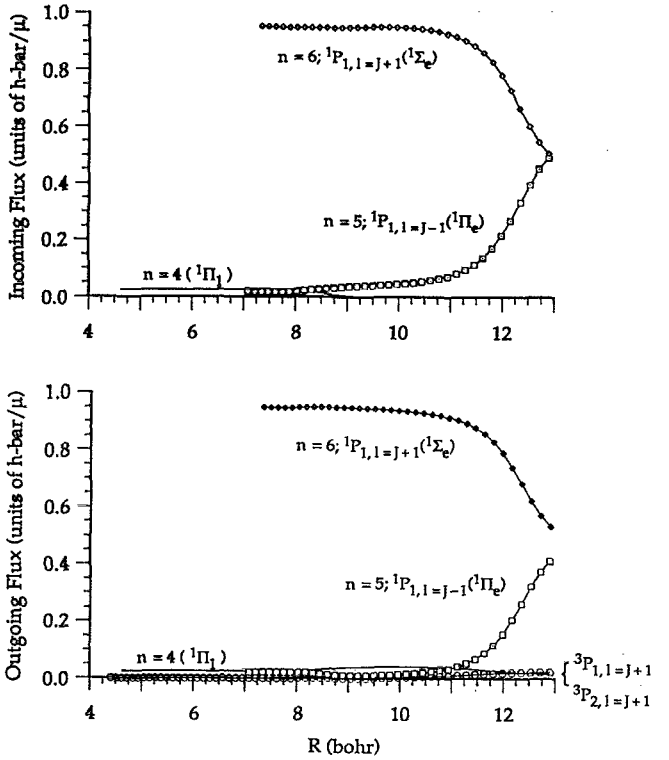


FIG. 5. (Upper panel) Redistribution of incoming flux among the various adiabatic $e$-labeled states of the Ca($4s5p\ ^{1,3}P$) He system (see Fig. 3) at an energy in the $^1P$ state of 540 $cm^{-1}$ and $J_{tot} = 10$. The initial state, with fluxes indicated by the open squares and open diamonds, is the linear combination of the two case (e) $^1P_e$ states which are produced when the electric field vector of the excitation laser is aligned *parallel* to the relative velocity vector; see Eq. (15). The fluxes in the various adiabatic states are plotted only up to the classical turning points for these states. The incoming flux in the $n = 1$, 2, and 3 states is negligibly small on the scale of the figure. (Lower panel) Identical to the upper panel except that the outgoing flux is plotted.

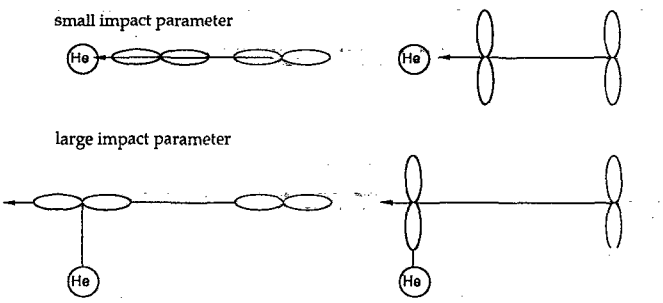


FIG. 6. Simplistic representation of the effect of initial orbital preparation in collsions of Ca($4s5p$). At small impact parameter, illustrated in the top two cartoons, excitation of the $5p$ orbital oriented *parallel* to the relative velocity vector will lead preferentially to population of the $^1\Sigma_e$ potential (Fig. 1) while excitation of the $5p$ orbital oriented *perpendicular* to the relative velocity vector will lead to population of the $^1\Pi_e$ potential. At large impact parameter, illustrated in the lower two cartoons, the situation is *reversed*: parallel excitation will lead to preferential population of the $^1\Pi_e$ potential and perpendicular excitation, to population of the $^1\Sigma_e$ potential. In reality, at large impact parameter considerable mixing of the asymptotically prepared states will occur because of the substantial rotational coupling between the $^1\Sigma_e$ and $^1\Pi_e$ states (Ref. 16).

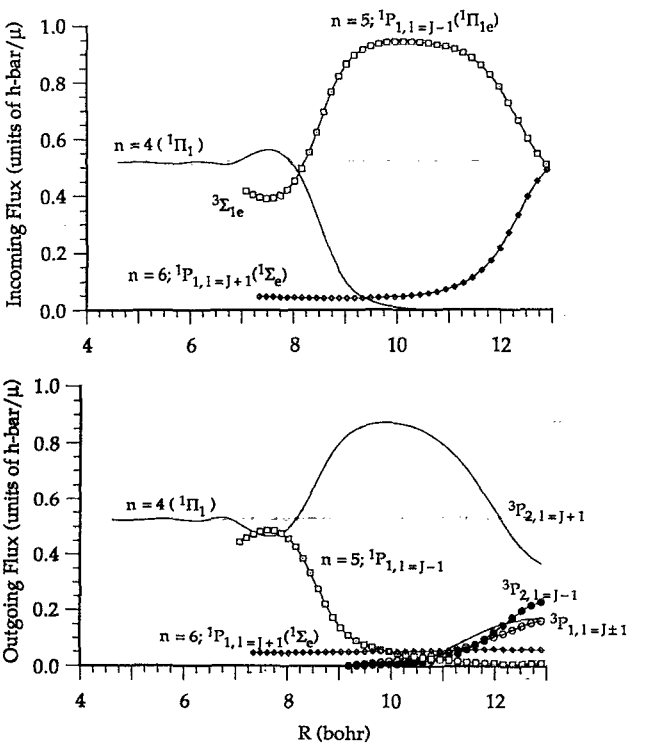


FIG. 7. (Upper panel) Redistribution of incoming flux among the various adiabatic $e$-labeled states of the Ca($4s5p\ ^{1,3}P$) He system (see Fig. 3) at an energy in the $^1P$ state of 540 $cm^{-1}$ and $J_{tot} = 10$. The initial state, with fluxes indicated by the open squares and open diamonds, is the linear combination of the two case (e) $^1P_e$ states which are produced when the electric field vector of the excitation laser is aligned *perpendicular* to the relative velocity vector; see Eq. (16a). Although at long range the $n = 5$ state can be described by the $^1\Pi_{1e}$ case (a) label, because of the curve crossing, at short range the same adiabatic state is described as $^3\Sigma_{1e}$. The fluxes in the various adiabatic states are plotted only up to the classical turning points for these states. The incoming flux in the $n = 1$, 2, and 3 states is negligibly small on the scale of the figure. (Lower panel) Identical to the upper panel except that the outgoing flux is plotted. For clarity, the small fluxes in the $^3P_{2,l=J-1}$ and $^3P_{2,l=J+1}$ states are plotted only for $R > 9$; at shorter internuclear distances the fluxes in these states are negligibly small.

transferred progressively to the $n = 5$ state which corresponds at short range to the case (a) $^1\Pi_e$ state, and subsequently into the $n = 4$ state, which correlates with the $^3\Sigma_{1e}$ state. By contrasting the upper panel of Fig. 7 with the upper panel of Fig. 4, we observe that the mechanism of $^1P \rightarrow {}^3P$ transfer as the Ca and He atoms approach is extremely similar in the case of perpendicular excitation, independent of the $e/f$ label of the initially excited state. The corresponding picture of the flux redistribution as the particles recede is displayed in the bottom panel of Fig. 7. As in the case of initial excitation of the $^1P_f$ state (Fig. 4), a significant redistribution of the triplet surface flux occurs as the particles recede through the radial coupling region. Here, however, comparison of the *lower* panels of Figs. 4 and 7 shows that the redistribution of flux among the $^3P_j$ states strongly depends on the $e/f$ label, primarily due to the presence of the unique $^3\Sigma_{0f}$ state.

The value of $J_{tot} = 10$ chosen for the analysis in this section corresponds to a maximum in the partial cross section curves for $^1P \rightarrow {}^3P$ transfer (Fig. 2). The succeeding minimum occurs at $J_{tot} = 16$. At $J_{tot} = 16$ the adiabatic potential curves are virtually unchanged from those displayed

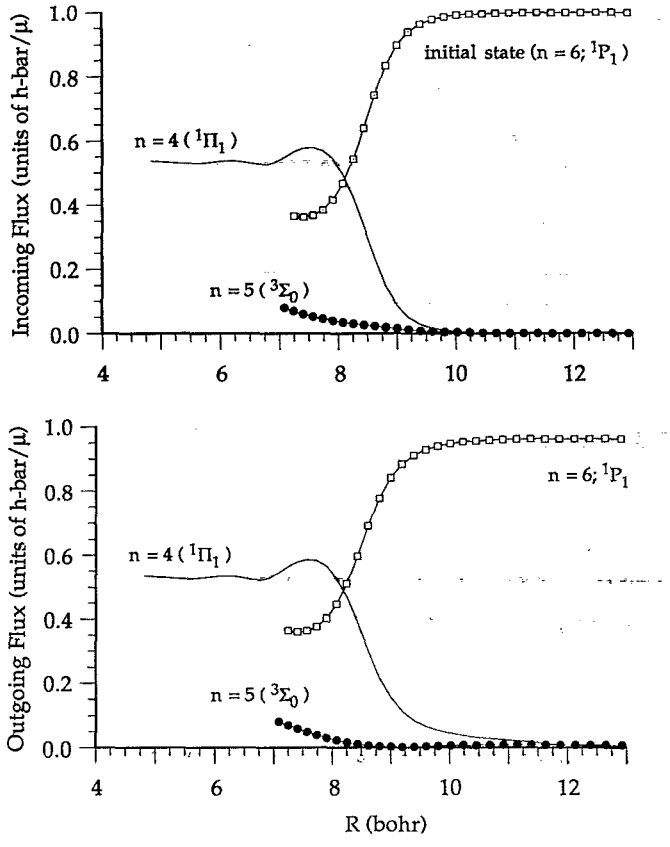


FIG. 8. (Upper panel) Redistribution of incoming flux among the various adiabatic *f*-labeled states of the Ca($4s5p\ ^{1,3}P$) He system (see Fig. 3) at an energy in the $^1P$ state of 540 cm$^{-1}$ and $J_{tot} = 16$. The initial state, with flux indicated by the open squares, is $n = 6$ ($^1P_{1f}$). The fluxes in the various adiabatic states are plotted only up to the classical turning points for these states. The incoming flux in the $n = 1$, 2, and 3 states is negligibly small on the scale of the figure. (Lower panel) Identical to the upper panel except that the outgoing flux is plotted.

## V. FLUX TRANSFER, LARGE IMPACT PARAMETER

In this section we consider collisions at a total angular momentum of $J_{tot} = 47$. This corresponds to the last maximum in the $^1P \rightarrow {}^3P_2$ partial cross sections shown in Fig. 2. The six adiabatic potential curves associated with the *e*-labeled levels are shown in Fig. 9. Because of the significantly larger centrifugal barrier, the curvature in the adiabatic potential curves is considerably reduced from that at $J_{tot} = 10$ (Fig. 3). The differences between the *e*- and *f*-labeled adiabatic curves are similar to what was seen at $J_{tot} = 10$ (Fig. 3); correspondingly we do not show the *f*-labeled curves for $J_{tot} = 47$.

Figure 10 displays the incoming fluxes corresponding to initial excitation of the $^1P_e$ state for $J_{tot} = 47$ and $E_{col} = 540$ cm$^{-1}$. These two figures correspond, respectively, to the situation in which the electric field vector is aligned *parallel* and *perpendicular* to the initial relative velocity vector. As illustrated in Fig. 6, on intuitive grounds one would expect that at large impact parameter, excitation of the $5p$ orbital initally lying perpendicular to the relative velocity vector should preferentially induce population of the $^1\Sigma_e$ curve (Fig. 1). Similarly, parallel excitation should induce preferential population of the $^1\Pi_e$ curve. We observe that this prediction of this intuitive picture are borne out by the flux calculations: In the case of perpendicular excitation (upper panel of Fig. 10) the incoming flux, split initially between the two $^1P_e$, $l = J \pm 1$ states, is transferred progressively to the $n = 6$ adiabatic state which corresponds at short range to the $^1\Sigma_e$ state. Consequently, transfer to the adiabatic states of triplet multiplicity is reduced as compared to parallel excitation (lower panel of Fig. 10), where flux is transferred progressively to the $n = 5$ adiabatic state which corresponds at short range to the case (a) $^1\Pi_e$ state.

in Fig. 3. When we examine the incoming and outgoing flux associated with initial excitation of the $^1P_f$ state at $J_{tot} = 16$, we observe (Fig. 8) that the incoming flux redistributes itself in a manner virtually identical to that found for $^1P_{1f}$ excitation for $J_{tot} = 10$ (Fig. 4), namely, transfer from the $^1P_{1f}$ state into primarily the $n = 4$ level, and, secondarily, into $n = 5$. However, the flux redistribution as the particles recede is dramatically different between $J_{tot} = 16$ and $J_{tot} = 10$; compare the lower panels of Figs. 4 and 8. As we have seen, at $J_{tot} = 10$, flux is transferred from the singlet to triplet states with equal probability as the particles approach and again as they recede. However, at $J_{tot} = 16$ the incoming and outgoing paths appear to be nearly reversible. All the flux gained by the $n = 4$ and $n = 5$ states as the particles approach is *returned* to the initial $n = 6$ level as the particles recede. The result is virtually zero net flux transfer from the $^1P_f$ state into the $^3P_f$ states. Figure 8 is the quantum analogue of the semiclassical picture[25,26] which attributes the minima in the partial cross sections (Fig. 2) to destructive interference between two trajectories one of which undergoes the $^1P \rightarrow {}^3P$ transition on the way in and the other, on the way out.

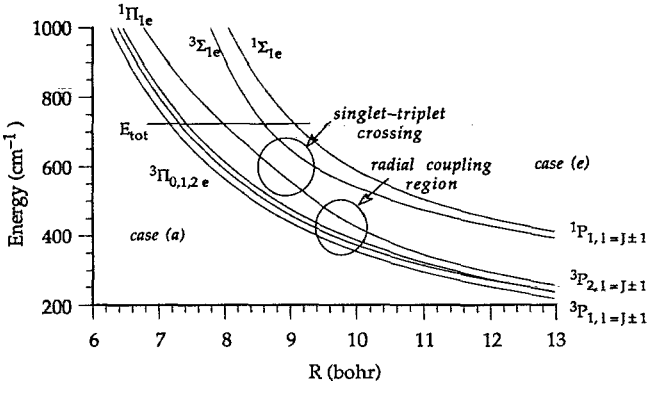


FIG. 9. Dependence on internuclear distance of the six *e*-labeled adiabatic potential curves for the collision of Ca($4s5p\ ^{1,3}P$) with He for $J_{tot} = 47$. The curves are designated by appropriate Hund's case (a) and case (e) labeling [valid at small and large $R$, respectively (see Refs. 2 and 36)]. The underlying electronic potential curves were taken from Ref. 2 and are shown in Fig. 1. The region of strong spin–orbit mixing between the $^1\Pi_{1e}$ and $^3\Sigma_{1e}$ curves is shown, as is the region of "radial coupling" (Refs. 26, 41, and 42) at which point the splitting between the $^3\Sigma$ and $^3\Pi$ curves becomes comparable to the fine structure splittings in the $^3P$ state of the isolated Ca atom. The horizontal line indicates the value of the total energy for which the flux analysis was carried out.

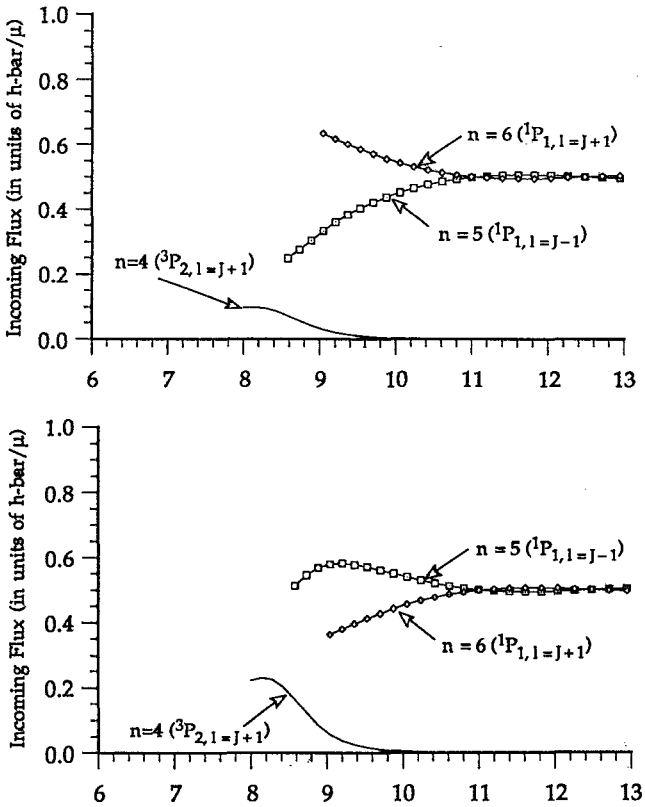


FIG. 10. (Upper panel) Redistribution of incoming flux among the various adiabatic *e*-labeled states of the Ca(4s5p $^{1,3}P$) He system (see Fig. 9) at an energy in the $^1P$ state of 540 cm$^{-1}$ and $J_{tot} = 47$. The initial state, with fluxes indicated by the open squares and open diamonds, is the linear combination of the two case (e) $^1P_e$ states which are produced when the electric field vector of the excitation laser is aligned *perpendicular* to the relative velocity vector; see Eq. (16a). The fluxes in the various adiabatic states are plotted only up to the classical turning points for these states. The incoming flux in the $n = 1$, 2, and 3 states is negligibly small on the scale of the figure. (Lower panel) Identical to the upper panel except that the electric filed vector of the excitation laser is aligned *parallel* to the relative velocity vector; see Eq. (15).

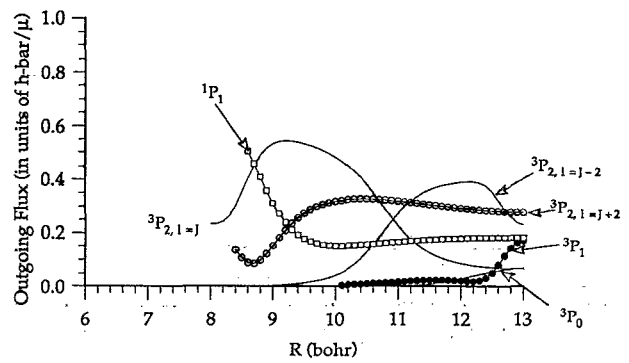


FIG. 11. Redistribution of *outgoing* flux among the various adiabatic *f*-labeled states of the Ca(4s5p $^{1,3}P$) He system (see Fig. 3) at an energy in the $^1P$ state of 540 cm$^{-1}$ and $J_{tot} = 47$. The initial state, with flux indicated by the open squares, is $n = 6$ ($^1P_{1f}$). The fluxes in the various adiabatic states are plotted only up to the classical turning points for these states.

We observe, however, that the variation is nowhere near as pronounced as was observed at small impact parameter (compare the upper panels of Figs. 5 and 7). This is because the rotational coupling between the $^1\Sigma_{1e}$ and $^1\Pi_{1e}$ states, whose magnitude varies with $J_{tot}$,[16] induces a far greater degree of mixing of the asymptotically prepared states at $J_{tot} = 47$.

The redistribution of the fluxes as the particles recede is illustrated schematically by Fig. 11, which shows the outgoing flux associated with initial excitation of the $^1P_{1f}$ state for $J_{tot} = 47$ and $E_{col} = 540$ cm$^{-1}$. Substantial redistribution of the populations in the triplet states takes place as the particles recede through the radial coupling region. We find an additional dramatic region of flux redistribution at larger $R$, which was not apparent at $J_{tot} = 10$. This additional coupling intervenes near the value of $R$ at which the $^3\Sigma$ interaction potential drops below the $^3\Pi$ potential at long range, due to the larger polarizability of the Ca(4s5p) atom when the 5p orbital is oriented along the Ca–He axis. We also observe that the degree of flux transfer to the $^3P_0$ state is larger at $J_{tot} = 47$ than at $J_{tot} = 10$. This is because the strength of the rotational coupling between the $^3\Pi_0$ and $^3\Pi_1$ states increases linearly with $J_{tot}$.[16] The redistribution of outgoing flux associated with initial excitation of the $^1P_{1e}$ state is qualitatively similar

## VI. CONCLUSION

We have applied here a new method for the fully quantum study of the dynamics of inelastic molecular collisions, which is based on the determination, as a function of interparticle separation, of the redistribution of the incoming inelastic flux among the various internal adiabatic states of the system. The application here to spin-changing collisions of Ca atoms, initially excited to the 4s5p $^1P$ state, allowed us to investigate, in a fully quantum manner, the dynamics of the transfer of flux to the nearby 4s5p $^3P$ state, and, subsequently, the redistribution of flux among the multiplet levels of the $^3P$ state. Conceptually, our approach is equivalent to placing a series of detectors along the reaction path, which can measure the distribution of the system among the internal states which are locally energetically accessible. These are flux, rather than number, detectors and are unidirectional, in that they are sensitive to the internal state distributions either as the collision partners approach or as they recede.

Application of this method to spin-changing collisions of Ca(4s5p) with He as a collision partner led to the following major conclusions: First, transfer from the initially excited singlet state to the triplet states occurs exclusively by means of the crossing between the $^1\Pi$ and $^3\Sigma_1$ curves. Secondly, the ultimate distribution of population among the fine-structure levels of the $^3P$ state is governed by couplings among the triplet states in the exit channel, as the particles recede, first through the "radial coupling" region,[26,41] where the splitting between the adiabatic curves of triplet multiplicity becomes equal to the fine-structure splittings in the isolated Ca atom. An additional coupling region, which becomes important as the total angular momentum increases, occurs at the long-range curve crossing between the $^3\Pi$ and $^3\Sigma$ curves.

The third major conclusion concerns the influence of

the polarization of the initially excited $5p$ orbital. For collisions at small impact parameter, the evolution of the flux associated with initial excitation of the $5p$ orbital lying along the relative velocity vector leads, at shorter distances, to virtually exclusive population of the $^1\Sigma_1$ state. Consequently, because the $^1\Sigma_1$ curve is not crossed by any curves of nominal triplet multiplicity, there is little flux transfer to the triplet states. On the other hand, initial excitation of the $5p$ orbital lying perpendicular to the relative velocity vector (but in the plane of the collision) leads, at shorter distances, to virtually exclusive population of the $^1\Pi_1$ state, with subsequent transfer of population to the triplet states. At large impact parameter the situation is reversed: flux transfer to the triplet states is enhanced by initial excitation of the $5p$ orbital lying parallel to the relative velocity vector and defavorized by initial excitation of the $5p$ orbital which lies perpendicular to the relative velocity vector.

The fourth major conclusion concerns the nature of the oscillatory structure observed in the partial cross sections for the spin-changing process. At the values of $J_{tot}$ corresponding to the relative *maxima*, transfer of flux from the singlet to triplet states appears to occur equally probably as the particles pass through the singlet–triplet crossing as they approach and then again as they recede. By contrast, at the values of $J_{tot}$ corresponding to the relative *minima*, the transfer of flux is *reversed* as the particles recede through the point of crossing.

As might be expected, all of the above mechanistic implications are fully consistent with the predictions of models based on semiclassical treatments of the collision dynamics. The advantage of the fully quantum treatment used here is the freedom from any inaccuracies or ambiguities which might arise from the separation of classical and quantum degrees of freedom (as, for example, is done in semiclassical impact parameter methods based on some average trajectory[44–47]).

One drawback of our earlier studies[1,2,5] on collisions of Ca($4s5p$) atoms is the reliance on model potentials. As *ab initio* potentials for the Ca($4s5p$) + noble gas systems become available,[39,40] the quantum flux analysis used here, along with the full close-coupling methodology outlined in our earlier papers,[1,2] will provide the means for future refinements of our full understanding of orbital polarization effects in inelastic collisions.

## ACKNOWLEDGMENTS

This research was supported by the U.S. Army Research Office, under Grant No. DAAL03-91-G-0129. The author is grateful to the Alexander von Humboldt Foundation for a Senior U.S. Scientist award during the tenure of which much of the work described here was carried out at the University of Bielefeld, Germany. Thanks are extended to Professor Brigitte Pouilly for helpful discussions and incisive comments on the manuscript.

[1] B. Pouilly and M. H. Alexander, J. Chem. Phys. **86**, 4790 (1987).
[2] B. Pouilly, J.-M. Robbe, and M. H. Alexander, J. Chem. Phys. **91**, 1658 (1989).
[3] L. J. Kovalenko, S. R. Leone, and J. B. Delos, J. Chem. Phys. **91**, 6948 (1989).
[4] G. C. Schatz, L. J. Kovalenko, and S. R. Leone, J. Chem. Phys. **91**, 6961 (1989).
[5] B. Pouilly and M. H. Alexander, Chem. Phys. **145**, 191 (1990).
[6] M. O. Hale and S. R. Leone, J. Chem. Phys. **79**, 3352 (1983).
[7] M. O. Hale, I. V. Hertel, and S. R. Leone, Phys. Rev. Lett. **53**, 2296 (1984).
[8] W. Bussert, D. Neuschäfer, and S. R. Leone, J. Chem. Phys. **87**, 3833 (1987).
[9] W. Bussert and S. R. Leone, Chem. Phys. Lett. **138**, 276 (1987).
[10] R. W. Schwenz and S. R. Leone, Chem. Phys. Lett. **133**, 433 (1987).
[11] S. R. Leone, in *Selectivity in Chemical Reactions*, edited by J. C. Whitehead (Kluwer Academic, Dordrecht, 1988), p. 245.
[12] F. H. Mies, Phys. Rev. A **7**, 942 (1973).
[13] V. Aquilanti and G. Grossi, J. Chem. Phys. **73**, 1165 (1980).
[14] V. Aquilanti, P. Casavecchia, G. Grossi, and A. Laganá, J. Chem. Phys. **73**, 1173 (1980).
[15] J. T. Hougen, Natl. Bur. Stand. (U.S.) Monogr. **115** (1970).
[16] H. Lefebvre-Brion and R. W. Field, *Perturbations in the Spectra of Diatomic Molecules* (Academic, New York, 1986).
[17] J. Grosser, J. Phys. B. At. Mol. Phys. **14**, 1449 (1981).
[18] H. W. Hermann and I. V. Hertel, Comments At. Mol. Phys. **12**, 61 (1982).
[19] R. Witter, E. E. Campbell, C. Richter, H. Schmidt, and I. V. Hertel, Z. Phys. D **5**, 101 (1987).
[20] J. Grosser, Z. Phys. D **3**, 39 (1986).
[21] M. H. Alexander, J. Chem. Phys. **94**, 8931 (1991).
[22] A. Arthurs and A. Dalgarno, Proc. R. Soc. London, Ser. A **256**, 540 (1960).
[23] W. A. Lester, Jr., Methods Comput. Phys. **10**, 211 (1971).
[24] See, for example, D. Secrest, in *Atom–Molecule Collision Theory: A Guide for the Experimentalist*, edited by R. B. Bernstein (Plenum, New York, 1979), p. 265.
[25] M. S. Child, *Molecular Collision Theory*, 2nd ed. (Academic, New York, 1974).
[26] E. E. Nikitin and S. Y. Umanskii, *Theory of Slow Atomic Collisions* (Springer-Verlag, Berlin, 1984).
[27] B. R. Johnson, J. Comput. Phys. **13**, 445 (1973).
[28] L. D. Thomas, M. H. Alexander, R. B. Walker, B. R. Johnson, W. A. Lester, J. C. Light, K. D. McLenithan, G. A. Parker, M. J. Redmon, T. G. Schmalz, and D. Secrest, J. Comput. Phys. **41**, 407 (1981).
[29] F. Mrugala and D. Secrest, J. Chem. Phys. **78**, 5954 (1983).
[30] F. Mrugala and D. Secrest, J. Chem. Phys. **79**, 5960 (1983).
[31] D. E. Manolopoulos, J. Chem. Phys. **85**, 6425 (1986).
[32] M. H. Alexander and D. E. Manolopoulos, J. Chem. Phys. **86**, 2044 (1987).
[33] R. G. Gordon, J. Chem. Phys. **51**, 14 (1969).
[34] R. G. Gordon, Methods Comput. Phys. **10**, 81 (1971).
[35] M. H. Alexander and B. Pouilly, in *Selectivity in Chemical Reactions*, edited by J. C. Whitehead (Kluwer Scientific Publishers, Dordrecht, 1988), p. 265.
[36] M. H. Alexander and B. Pouilly, J. Chem. Phys. **90**, 5373 (1989).
[37] D. M. Brink and G. R. Satchler, *Angular Momentum*, 2nd ed. (Clarendon, Oxford, 1968).
[38] J. M. Brown, J. T. Hougen, K.-P. Huber, J. W. C. Johns, I. Kopp, H. Lefebvre-Brion, A. J. Merer, D. A. Ramsay, J. Rostas, and R. N. Zare, J. Mol. Spectrosc. **55**, 500 (1975).
[39] E. Czuchaj, F. Rebentrost, H. Stoll, and H. Preuss, Chem. Phys. **138**, 303 (1989).
[40] E. Czuchaj (to be published).
[41] E. E. Nikitin, J. Chem. Phys. **43**, 744 (1965).
[42] E. E. Nikitin, in *Chemische Elementarprozesse*, edited by H. Hartmann (Springer, Berlin, 1968).
[43] C. E. Moore, *Atomic Energy Levels*, NSRDS-NBS 35 (U.S. Government Printing Office, Washington, D.C., 1971).
[44] T. F. Moran, M. R. Flannery, and P. C. Cosby, J. Chem. Phys. **61**, 1261 (1974).
[45] T. F. Moran, K. J. McCann, M. Cobb, R. F. Borkman, and M. R. Flannery, J. Chem. Phys. **74**, 2325 (1981).
[46] A. E. DePristo, J. Chem. Phys. **78**, 1237 (1983).
[47] B. M. Rice, B. C. Garrett, P. K. Swaminathan, and M. H. Alexander, J. Chem. Phys. **90**, 575 (1989).